Plant Cell Reports (2023) 42:1571–1587
https://doi.org/10.1007/s00299-023-03048-z

ORIGINAL ARTICLE

Size variations of mesoporous silica nanoparticle control uptake efficiency and delivery of *AC2*-derived dsRNA for protection against tomato leaf curl New Delhi virus

Anju Sangwan[1] · Dipinte Gupta[2] · Oinam Washington Singh[2] · Anirban Roy[2] · Sunil Kumar Mukherjee[2] · Bikash Mandal[2] · Neetu Singh[1,3]

Received: 23 October 2022 / Accepted: 7 July 2023 / Published online: 24 July 2023

Abstract

Key message **We report the size dependent uptake of dsRNA loaded MSNPs into the leaves and roots of *Nicotiana benthamiana* plants and accessed for their relative reduction in Tomato leaf curl New Delhi viral load.**

Abstract A non-GMO method of RNA interference (RNAi) has been recently in practice through direct delivery of double stranded RNA into the plant cells. Tomato leaf curl New Delhi virus (ToLCNDV), a bipartitie begomovirus, is a significant viral pathogen of many crops in the Indian subcontinent. Conventional RNAi cargo delivery strategies for instance uses viral vectors and Agrobacterium-facilitated delivery, exhibiting specific host responses from the plant system. In the present study, we synthesized three different sizes of amine-functionalized mesoporous silica nanoparticles (*amino*-MSNPs) to mediate the delivery of dsRNA derived from the *AC2* (dsAC2) gene of ToLCNDV and showed that these dsRNA loaded nanoparticles enabled effective reduction in viral load. Furthermore, we demonstrate that *amino*-MSNPs protected the dsRNA molecules from nuclease degradation, while the complex was efficiently taken up by the leaves and roots of *Nicotiana benthamiana*. The real time gene expression evaluation showed that plants treated with nanoparticles of different sizes ~ 10 nm ($MSNP_{DEA}$), ~ 32 nm ($MSNP_{TEA}$) and ~ 66 nm ($MSNP_{NH3}$) showed five-, eleven- and threefold reduction of ToLCNDV in *N. benthamiana*, respectively compared to the plants treated with naked dsRNA. This work clearly demonstrates the size dependent internalization of *amino*-MSNPs and relative efficacy in transporting dsRNA into the plant system, which will be useful in convenient topical treatment to protect plants against their pathogens including viruses.

Communicated by Om Parkash Parkash Dhankher.

✉ Bikash Mandal
leafcurl@rediffmail.com

✉ Neetu Singh
sneetu@cbme.iitd.ac.in

[1] Centre for Biomedical Engineering, Indian Institute of Technology Delhi, Hauz Khas, New Delhi 110016, India

[2] Advanced Centre for Plant Virology, Division of Plant Pathology, Indian Agricultural Research Institute, New Delhi 110012, India

[3] Biomedical Engineering Unit, All India Institute of Medical Sciences, Ansari Nagar, New Delhi 110029, India

Graphical abstract

Mesoporous silica nanoparticles loaded with FITC, checked for its uptake into *Nicotiana benthamiana*.

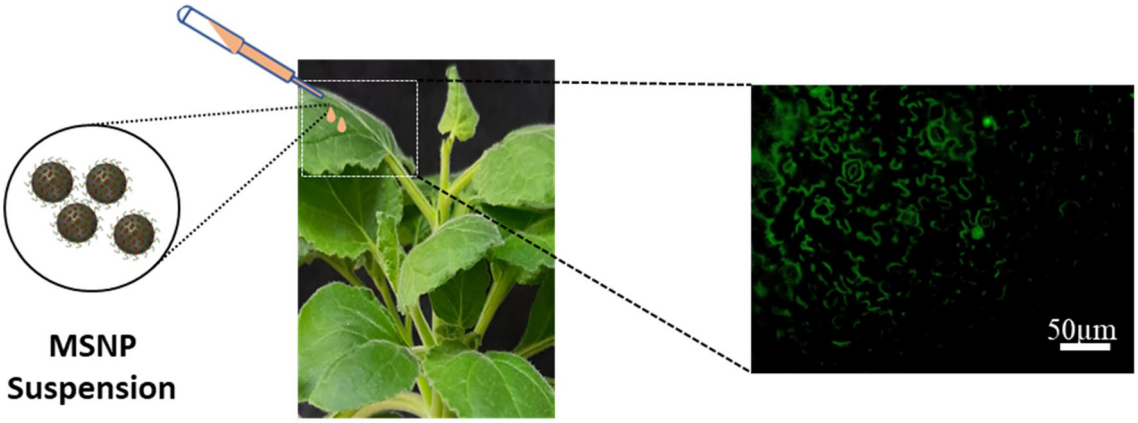

Mesoporous Silica Nanoparticles loaded with FITC, checked for its uptake into *Nicotiana benthamiana*

Keywords Mesoporous silica nanoparticles · dsRNA · ToLCNDV · Gene silencing · *AC2* gene · Topical application · Delivery systems

Introduction

As the world's human population is expanding, the food security poses a worldwide challenge due to growing food consumption and declining food production on account of unavailability of agrarian land, high transmission of plant diseases and ever-changing climatic conditions. To encounter the growing requirements of the expanding population of the world, the production of food needs to be double by 2050. Ever-evolving plant viruses pose a major threat to sustainable agriculture by affecting major crop production losses globally (Calil and Fontes 2017; Miller et al. 2017). An estimated loss of 10–15% of total world crop production is attributable to plant diseases (Strange and Scott 2005) and virus responsible for 47% of the plant diseases, causing billions of dollars in damage, retaining millions of people with hunger and malnutrition (Jones 2021; Boualem et al. 2016). Usually, plant viruses transmission from one plant to another involves a vector. Majority of the viruses are insect transmitted (Fiallo-Olivé et al. 2020). One of the most significant plant viruses, the *Tomato leaf curl New Delhi virus* (ToLCNDV, genus *Begomovirus,* family *Geminiviridae*), which is vectored by whiteflies, affects the major economically essential crop, tomato, in the Indian sub-continent, constraining tomato production (Sharma and Prasad 2020). ToLCNDV, till date is the only bipartite begomovirus that cause infections in a variety of plants belonging to various families including Fabaceae, Euphorbiaceae, Malvaceae, Cucurbitaceae, and prominently Solanaceae (Moriones et al. 2017).

Conventional strategies using frequent use of broad-spectrum pesticides and insecticides, increase eventually insect vector resistance, thus posing a threat associated with environmental degradation and raise alarms for human health (Sharma et al. 2019). Hence, there is a pressing need for sustainable production strategies in global agriculture for the control of plant viral epidemics, that will ensure increase in crop yield per unit of cultivable land and remove adverse environmental effect (Bailey-Serres et al. 2019). Current attempts focus on using less amounts of fertilizers and pesticides, thereby amplifying crop yields sustainably. Newly emerged approaches that either directly or indirectly interferes with the propagation of viruses within their vectors include improvement of vector-associated immune control, exploitation of the vector microbiome, transgenic crops (Tabashnik and Carrière 2017), or usage of novel gene-editing techniques such as CRISPR–Cas9 systems (Douglas 2018). These approaches have gained lots of attention during the last decade, however, these strategies suffer from several limitations i.e., time-consuming, and tedious protocols, off-targeted toxicity, unwanted gene integration within host plant, unsustained release of the biomolecules (nucleotides, proteins) and low transformation efficiencies. Hence, there is ever rising demand of innovative approaches for high production with lesser toxicity and ethical concerns.

Among several disease management approaches adopted, RNA interference (RNAi) has drawn attention because

of its robust resistance against viral pathogens and pests, practical achievability, and low cost in comparison to other genetic engineering approaches (Zotti et al. 2018; Darsan Singh et al. 2019; Mohan et al. 2021). RNAi is a regulatory mechanism of modulating gene expression by dsRNAs that are recognised by the target or homologous mRNA in the cells. Mechanistically, dsRNA is cleaved by DICERs into small RNAs, which are then incorporated into RNA Induced Silencing Complex (RISC) that degrades the homologous RNA leading to decrease in the gene expression. Thus, water-soluble preparations containing dsRNA/siRNA against viral pathogens can also act as sprayable antiviral substitutes for cases in which plant genetic transformation is not feasible or highly expensive. Despite its high potential in controlling diseases, limitations such as easy degradation of naked dsRNA and uptake restrictions by plant cells has made such exogenous RNAi really challenging for achieving success in plants. The multilayer thick cellulosic cell wall acts as a barrier and not only constrains the delivery of biomolecules but also limits the application of other abiotic delivery approaches to plants. In contrast, abiotic approaches such as use of positively charged polymers, cationic lipids, electroporation, and heat shock are commonly used in mammalian systems. Viral vectors and *Agrobacterium*-mediated transformation are the preferred approaches to deliver siRNA into intact plant cells. Viral vectors delivering siRNA/dsRNA, allows strong siRNA/dsRNA expression without relying on plant's transformation (Zhang et al. 2021). However, majority of the viruses have specific host range, need taming of pathogenicity, and also such approaches require the cDNA insertion/construction into the viral vectors etc., often resulting in inconsistent gene silencing. Moreover, Agrobacterium-mediated transformation, the other generic method for applying RNAi in plants, is also constrained to few particular plant species and can adversely and unpredictably affect the cell operation caused by random DNA integration during transformation, resulting in plant's endogenous gene disruption or constitutive expression of the siRNA (Demirer et al. 2020).

One promising tool to overcome these limitations is the use of nanoparticle-based dsRNA/siRNA delivery systems as exogenous applications to plants (He et al. 2013). The agronomical application of nanotechnology can overcome conventional delivery system for plants allowing improved efficacy (Ghassemi-Golezani and Abdoli 2021), stimuli-controlled release (Abdo et al. 2020), targeted delivery (Kwak et al. 2019), and reduced dosage (Wang et al. 2019). In the last decade, various engineered nanoparticle (ENP) systems have been developed for RNAi cargo in agriculture against pests and pathogens, such as chitosan nanoparticles (Das et al. 2015), gold nanoparticles (AuNPs) (Lei et al. 2020), carbon nanotubes (Demirer et al. 2020), layered double hydroxides (LDH) nanosheets (Mitter et al. 2017; Worrall et al. 2019) and Mesoporous silica nanoparticles (MSNPs) (Niazian et al. 2021). The physio-chemical properties of NPs, such as size, charge, low water dispersibility, composition, low loading capacities, low, difficulties in high scale production and controlled synthesis, may deter their potential application into drug delivery. Also, delivering drugs to plants is primarily dependent on xylem capillary action (especially in roots) and diffusion. Thus, nanoparticle size and surface charge may play a key role in transport through the plant cells and tissues (Palocci et al. 2017). Hence, we hypothesized that an efficient system can be identified by developing nanoparticles with varying sizes and surface properties. Also, we envisioned hard inorganic nanoparticles compared to polymeric nanoparticles might be better as it can withstand mechanically harsh methods of application i.e., rub inoculation, etc. Mesoporous silica nanoparticles (MSNPs) were chosen for developing the RNAi platform as it offers remarkable advantages such as biocompatibility, large surface area (often more than 1000 m^2/g), a solid framework of tunable pore size and easily controllable surface chemistry and functionalization compared to other nanoparticle systems (Tarn et al. 2013). In addition, mild synthetic protocol that can be translated into large-scale production and yields optimal size with low polydispersity and drug release gating mechanism makes it a unique and potential drug delivery system for plant cells (Tarn et al. 2013; Sun et al. 2014; Narayan et al. 2018).

In this work, as illustrated in Scheme 1, we synthesized three different sizes of MSNPs with average sizes *i.e.* < 10 nm ($MSNP_{DEA}$), < 50 nm ($MSNP_{TEA}$) and < 80 nm ($MSNP_{NH3}$), loaded them with dsRNA targeting *AC2* gene of ToLCNDV and subsequently studied delivery into plant leaf and root tissues. *AC2* was chosen as the target region for RNA silencing, because protein associated with *AC2* interacts with host kinases and impairs plant innate transcriptional (TGS) and post-transcriptional gene silencing (PTGS) process (Sharma et al. 2015; Rahman et al. 2021). All three MSNPs have shown uptake and provided systemic viral protection in the experimental host *Nicotiana benthamiana.* To the best of our knowledge, MSNPs have not yet been reported to serve as dsRNA delivery agents in knock-down of plant viruses.

Materials and methods

Materials

N-cetyltrimethylammonium bromide (CTAB), tetraethylorthosilicate (TEOS), 3-aminopropyltriethoxysilane (APTES), ammonia solution 25%, Rhodamine-B were purchased from Sigma-Aldrich. Diethanol amine (DEA), Triethanol amine (TEA) and all

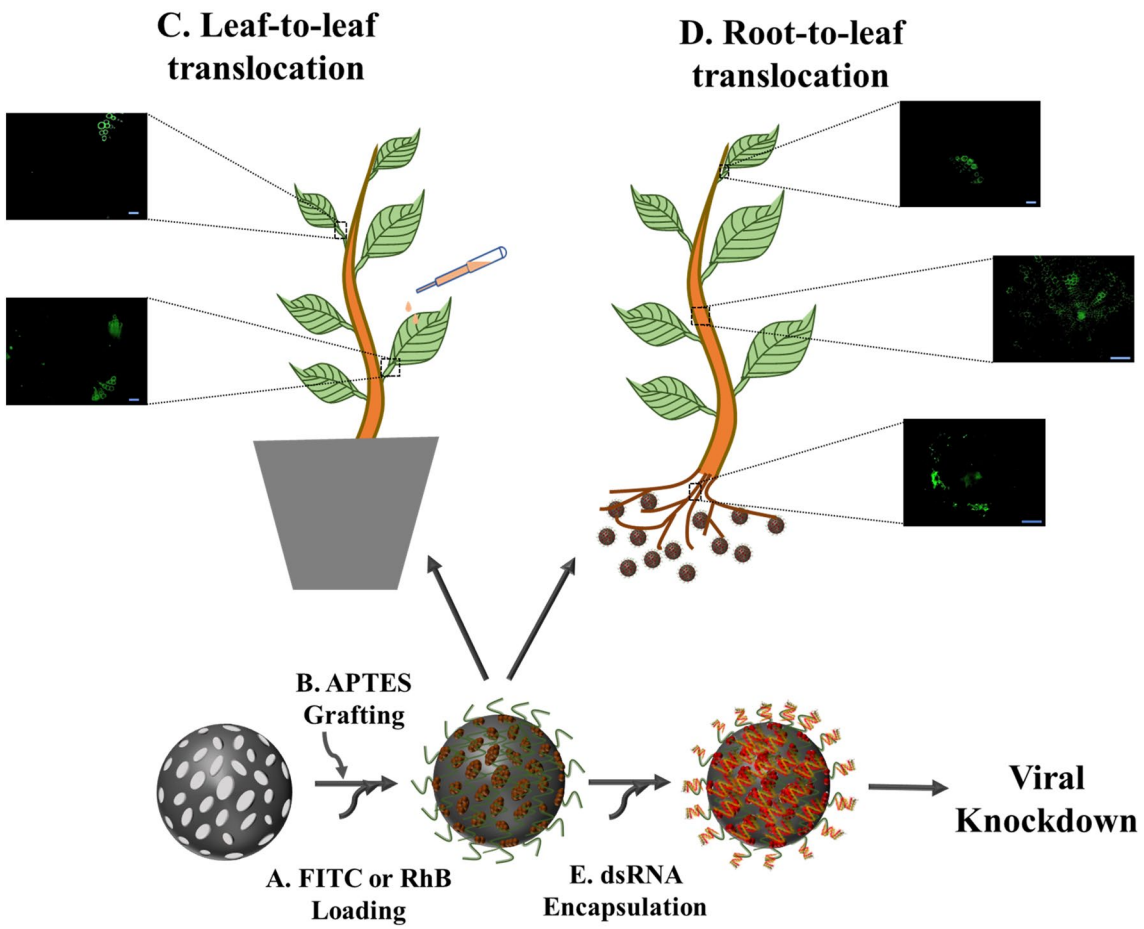

Scheme 1 Schematic representation of mesoporous silica nanoparticles (MSNPs). **A** Loading of Rhodamine-B or FITC followed by **B** amine functionalization of the silica surface with APTES making it positively charged surface and assessed for internalization by the plants (**C** rub inoculation, **D** by dipping the roots into MSNP solutions), afterwards, (E) encapsulating the dsRNA cargo, finally the efficacy of dsRNA conjugated MSNPs has been analyzed

chemicals were of analytical grade and were used without further purification. Deionized (DI) water from HiMedia Laboratories was used throughout the experiments. Experimental plant *Nicotiana benthamiana* were used for the uptake and knockdown experiments.

dsRNA preparation

Full-length *AC2* gene (419 bp) of ToLCNDV was amplified by using gene-specific primers (Supplementary Table 2). The PCR-ampified product were cloned in TA vector (pTZ57R/T) and sequenced. Further, the AC2 insert was ligated in L4440 vector, which has IPTG inducible bacterial T7 promoter at both ends. The recombinant plasmid was added to transform HT115 bacterial strain (an RNase III mutant strain of *E. coli*). dsRNA was extracted from the HT115 cells by using Tri-xtract reagent as described in Singh et al (2022) and stored at −20 °C for further use. The dsRNA concentration was estimated spectrophotometrically (Nabi-μ^2 Microdigital Co. Ltd NanoDrop, Thermo Fisher Scientific, United States) and quality was checked via gel electrophoresis.

Synthesis and characterization of nanoparticles

Preparation of different sizes of MSNPs

The modified Stober method was used to prepare MSNPs of various sizes (Wu and Lin 2013). First, CTAB was added to the deionized water and maintained under stirring for 10 min. Afterwards, base catalyst DEA, TEA and NH_3 was added to the solution, subsequently forming the $MSNP_{DEA}$, $MSNP_{TEA}$ and $MSNP_{NH3}$, respectively. TEOS was added dropwise by constant flow rate of 50 ml/h under continuous stirring. Then, the solution was left for stirring at room temperature for 24 h. The solution was centrifuged at 8000 rpm and washed three times with deionized water and ethanol. Then, the solvent extraction was carried out for 24 h

by refluxing as prepared MSNPs into 160 ml of methanol to which 9 ml of conc. HCL was added and kept at 80 °C to remove the surfactant. The base catalysts and amount of CTAB were varied to get different sizes, (supplementary Table 1). Finally, the resultant powders were redispersed in 100 ml of D.I. water for 12 h and later centrifuged and lyophilised to get final powdered samples.

Preparation of Rhodamine B and FITC-tagged silica nanoparticles (Rh-MSNPs)

2 mg of Rhodamine B was dispersed into 50 ml of deionized water under continuous stirring at 25 °C. After 15 min, 0.05 g of as synthesized MSNPs were added into solution and stirred for 50 min. Afterwards, solution was centrifuged and resulting nanoparticles washed thoroughly with deionized water. The concentration of supernatant was determined by UV–Vis at 554 nm.

For nanoparticle translocation study, MSNPs were tagged with Fluorescein isothiocyanate (FITC). 100 mg of MSNPs were suspended into 30 ml of absolute ethanol containing 200 µl of APTES and kept on stirring for 1 h. 2 mg of FITC dissolved in 10 ml of ethanol and added dropwise to the above mixture. After 2 h, 0.4 ml of D.I. water added to the mixture, keeping it on stirring for 24 h. Afterwards, solution was centrifuged and resulting nanoparticles washed thoroughly with ethanol and deionized water. The absorption and fluorescence spectra have been recorded at 488 and 519 nm wavelength.

Preparation of amine-functionalized MSNPs (*amino*-MSNPs)

100 mg of Rh-MSNPs was suspended in 20 ml of toluene containing 0.2 ml of APTES. The solution is stirred under reflux for 8 h at 60 °C. Then, solution is cooled down, centrifuged at 8000 rpm, and washed two times with toluene, two times with ethanol and finally washed with water.

Characterization of MSNPs

The synthesized nanocarriers were thoroughly characterized for their size, charge, and other intrinsic properties by High Resolution Transmission electron microscopy (HR-TEM), Field Emission scanning electron microscopy (FESEM), Zeta, Small Angle X-ray Scattering (SAXS), Low-angle Powder XRD (LAXRD), High angle Powder XRD (HAXRD), FTIR spectroscopy, BET Surface Area analysis, etc. HRTEM images were obtained from Tecnai™ G2 Twin (200 kV) FEG. The HRTEM images also served to calculate the particle size distributions, for which 100 particles were considered. The FESEM images were obtained on Jeol JSM-7800F Prime (Jeol Japan) from FEI operated at 10.0 kV with gold coating for 5 min. Zeta potential measurements were conducted on a Malvern Zetasizer Nano-series. Fourier-transform infrared (FTIR) absorption spectra were recorded on a Thermo electron scientific FTIR Spectrometer. Rhodamine-B calibration curve in water and loading capacity of MSNPs is obtained from UV–vis spectroscopy using SYNERGY H1 microplate reader from Biotek. Nitrogen physiosorption isotherms were measured at 77 K using a surface area analyzer (AUTOSORB-iQ XR) from Quantachrome with preheating time of 300 min at 100 °C. Low-angle powder X-ray diffraction pattern of the MSNP materials were obtained using an Empyrean X-ray Diffractometer (Malvern panalytical) using Cu K radiation ($\lambda = 0.154$ nm) and in the 2Θ range of 0°–5° and high angle powder X-ray diffraction pattern of the MSNP materials were obtained using a X'Pert PRO (PANalytical Netherlands) using Cu K radiation ($\lambda = 0.154$ nm) and in the 2Θ range of 10°–50° in a continuous mode. SAXS data obtained from SAXS point 2.0 (Anton Paar) with Cu X-ray source. Double-logarithmic plot has been plotted from SAXS patterns of MSNPs. Prepared dsRNA concentration was measured by using UV–Vis spectrophotometer (Nabi-μ^2 Microdigital Co. Ltd.). Nanoparticle uptake was assessed by using Leica Confocal Microscope.

In vitro cytotoxicity assays

The mammalian cell toxicity of the MSNPs was evaluated by (3-[4,5-dimethylthiazol-2-yl]-2,5 diphenyl tetrazolium bromide (MTT) assay and live-dead staining assay using calcein-AM and propidium iodide, respectively. For these assays, NIH 3T3 cells, a murine fibroblast cell line, were used. Cells were cultured in DMEM with 10% FBS and 1% anti solution at 37 °C in a CO_2 incubator (5% CO_2, 95% humidity). Once the cells reached a confluency of 80%, they were trypsinized and seeded at a density of 5000 cells/well in a 96-well plate. After 24 h of seeding, the samples were added into the wells at different concentrations (0.1, 0.08, 0.06, 0.04 and 0.02 mg/ml) and incubated for 24 h. After 24 h of incubation, to test the cytotoxicity of the nanoparticles, the MTT assay was performed as per manufacturer's protocol and the absorbance was measured at 595 nm. To further check the viabilities of the cells, the live-dead cell assay was also performed by Calcein-AM/PI staining. For this, after 24 h of incubation with nanoparticles, supernatant was removed, and cells were washed with media followed by addition of calcein and propidium Iodide. After 15 min of incubation, cells were imaged with an Olympus IX fluorescence microscope.

dsRNA conjugation with *amino*-MSNPs

About 10 mg of MSNPs was added in 10 ml of ethanol to make a suspension by sonicating it for 10 min. In an

eppendorf tube, 200 µl of the suspended solution was taken and ethanol was evaporated in oven at 60 °C. After complete evaporation, the sample was kept into UV light for 1 h for sterilization. Then, 30 µg of dsRNA was added and the complete volume was made to 100 µl by adding RNase free water followed by vigorous shaking and incubation for 24 h at 4 °C. The prepared complexes were centrifuged at 10,000 rpm for 10 min at 4 °C and washed three times with RNase free water to remove unloaded dsRNA and supernatent was collected. The dsRNA conjugation efficiency in the a*mino*-MSNPs was investigated by measuring the concentration of dsRNA in the supernatant spectrophotometrically. Conjugation efficiency (CE) of all three nanoparticles were calculated by following equation:

$$\mathrm{CE}(\%) = (A - B) / A \times 100,$$

where A is concentration of dsRNA used for conjugation, B is the concentration of unconjugated dsRNA in the supernatent.

The dsRNA loading ability of the a*mino*-MSNPs was assessed by gel retardation assay. To define optimal and complete loading of respective dsRNA onto nanopaticles, dsRNA with different concentrations; 100 µg/mg, 150 µg/mg and 200 µg/mg of nanoparticles was assayed multiple times. After formation of dsRNA nanocomplexes as described, dsRNA loading was checked by gel electrophoresis by retention of dsRNA–MSNP complexes in the well of a 1.2% agarose gel and visualized under a UV illuminator (Uvitec).

Nanoparticle uptake and localization of MSNPs in N.b. plants

All three MSNPs complexes were administered onto the *N. benthamiana* leaf surface by rub inoculation and into roots by soaking in NP solution. Uptake experiments were carried out at a concentration of 0.5 mg/mL. The roots of 1-month-old N.b. plants was submerged in 1.5 mL of nutrient solution containing 0.5 mg/mL MSNP-RhB or MSNP-FITC solution held in a 2-mL eppendorf tube and allowed to absorb the nanoparticle solutions for 1 h and then washed vigorously with water. To determine the ability of MSNPs to adhere, absorb and translocation, the absorption was tracked using Zeiss Inverted Fluoresecnce Microscopy and Zeiss LSM 70 Confocal Microscopy. The root, stem and petiole from the nanoparticle-exposed plants were embedded in 5% agarose and cross-sectioned into 80–100 µm under an oscillating tissue slicer (PELCO tissue slicer, Ted Pella). The sections were placed on a glass slide covered with 60% glycerol, then observed and imaged using inverted fluorescence microscope (Zeiss). The cross-sections were screened for FITC (490–525 nm wavelength) fluorescence.

In other experiment, the leaf of N.b. plants were exposed to MSNP-FITC solution by rub application. The plants were then placed in a plant growth chamber in dark for 24 h. Leaf midrib and petiole cross-sections of the treated and adjacent untreated leaves are taken and imaged using inverted fluorescence microscope (Zeiss). Also, foliar delivery efficiency has been checked by spraying plant leaves with all three nanoparticles and kept in incubation for 4 h. Leaves were vigrously washed and leaf disks of 4 mm were taken for nanoparticle localization, and imaged using inverted fluorescence microscope.

Plant sample preparation for transmission electron microscopy

N.b. plant roots were exposed to all three MSNPs at a density of 0.2 mg/mL and the nutrient solution containing no MSNPs wa used as the control. The root and leaf of plants were cut into 2 × 2 mm size. Immediately samples were fixed into a mixture of 2% Paraformaldehyde and 2.5% glutaraldehyde in 0.1 M phosphate buffer, first at room temperature for 20 min and later incubated at 4 °C overnight. The next day, samples were washed in buffer for 3 times, each for 1 h duration at 4 °C. Then, samples were post-fixed into 1% (v/v) osmium tetroxide in PB for 1 h. after that samples washed again with PB (1–2 h) to remove excess osmium tetroxide. Samples were dehydrated in graded acetone solutions (30%, 50%, 70%, 90%, 95%, absolute acetone, 15 min in each step). The specimens were then infilterated into a mixture of toulene and resin in 3:1 (1 h), 2:2 (1 h), 1:3 (1 h) ratios and then finally into pure resin (1 h, 2 changes). Finally, put the specimen overnight in embedding medium (Araldite CY212—10 ml, DDSA—8 ml, MNA—2 ml, DMP 30—0.4 ml) at 50^0C. Afterwards, increase the temp to 60 °C, for 60–72 h. Finally, Blocks are ready and the ultrathin sections (~80 nm) were attained with an ultramicrotomy (Ultramicrotome UC6) and post-stained with uranyl acetate and lead citrate. TEM images were obtained with a JEM-1400 (JEOL, Japan) operating at an accelerating voltage of 80 kV.

Plant growth conditions

Seeds of *N. benthamiana* were grown in a growth chamber at 24 ± 2 °C and 16/8 h of light and darkness periods, with 65% average humidity. All plant experiments were performed with attached leaves on 4 to 5 week old plants.

Agroinoculation, dsRNA and dsRNA-MSNPs treatment

Agrobacterium strain LBA4404 that consists of partial tandem dimers of DNA-A and DNA-B of ToLCNDV

and DNA-β of CYVMV were grown on LB medium replinished with Rifamcin and Kanamycin at 28 °C for overnight, with continuous shaking at 200 rpm. Then, the cells were collected after centrifuged at 6000*g* for 5 min and resuspended in 2-(*N*-morpholino)ethanesulfonic acid (MES) buffer till the OD_{600} reaches 0.8 and kept on 28 °C for 4 h at 80 RPM. All three cultures were mixed in a equal volume before agroinoculation. *N. benthamiana* plants were agroinfilterated with ToLCNDV(A + B) + CYMV β on the abaxial surface with 2.5 ml syringe on the three marked leaves. Plants were agroinfilterated with ToLCNDV only (Treatment 1), ToLCNDV + dsAC2 (Treatment 2), ToLCNDV + dsAC2-$MSNP_{DEA}$ (Treatment 3), ToLCNDV + dsAC2-$MSNP_{TEA}$ (Treatment 4) and ToLCNDV + dsAC2-$MSNP_{NH3}$ (Treatment 5). dsAC2 and dsAC2-MSNP complex suspension were applied on same three marked leaves (adaxial surface) by rubbing 15 µg of dsRNA and 15 µg/200 µg of nanoparticles per plant, respectively. Plant infiltrated with only methylmalonic acid (MMA) bufer were used as buffer control. Three experiments were analyzed independently for all treatments ($n = 3$ plants per treatment). After treatment with dsAC2 or MSNP-dsAC2 suspension, the relative levels of viral load were checked by qPCR of partial CP DNA by using the coat protein primers (BM1060 and BM1223) and actin was taken as the internal control (Li et al. 2018; Liu et al. 2022).

Stability of dsRNA from nucleases

Integrity of conjugated dsRNA with MSNPs is assessed by adding RNase and checked via gel electrophoresis (RNA protection gel assay). Protection capacity of dsRNA-loaded MSNPs were assessed in the presence of the RNase A (10 µg/µl) for 20, 40, 60, and finally 90 min. Gel analysis revealed that MSNPs are effective against protection for the loaded dsRNA against RNase treatment. Also, the competitive binding of nanoparticle and dsRNA were also analyzed using negatively charged Heparin. We had found the release of dsRNA from nanoparticle on adding heparin (4 mg/ml) at 2-min incubation.

Viral load and symptom reduction in plants

Post treatment, plants were regularly observed for the disease incidence and symptom development. Disease incidence index (%) has been calculated by counting the numbers of infected leaves out of 70 leaves among the treated plants. The ability of dsRNA-MSNP complex to afford systemic protection was assessed on new unsprayed leaves of *N. benthamiana* that emerged post spray in triplicates. Systemic leaves were taken at different intervals of time; day 6, 18 and 30th and assessed by qPCR for the relative quantification of viral load. Double C_t method was used to calculate the relative viral titres in all treated plants, equating the viral load as 1 unit in the untreated plants (Livak and Schmittgen 2001; Schmittgen and Livak 2008). For all the qPCR experiments, three technical replicates were used.

Statistical analysis

Experiments were performed in triplicates and analysis were carried by one-way ANOVA, and p value ≤ 0.05 was considered as statistically significant.

For qPCR analysis, all the treatment combinations were evaluated as independent experiments and ANOVA was used, p value ≤ 0.05 considered as statistically significant.

Results

Synthesis and characterization of MSNPs

Three different sizes of MSNPs were synthesized by modified stober method taking TEOS as silica source in the presence of three different type of base catalysts *i.e.* DEA, TEA and NH_3. The different ratio of reactants and types of base catalyst used in the reaction allowed us to tune the sizes. The size of MSNPs could be controlled in a range of 10 to 80 nm by various additive agents that control the hydrolysis and condensation of silicates during the synthesis (Narayan and Nayak 2018). Figure 1a–c shows the size of nanoparticles as confirmed by HR-TEM and FE-SEM. The average size was calculated by ImageJ, and observed to be ~ 10 ± 1 nm for $MSNP_{DEA}$, 32 ± 3 nm for $MSNP_{TEA}$ and 66 ± 6 nm for $MSNP_{NH3,}$ respectively. Figure 1d shows that the $MSNP_{DEA}$, $MSNP_{TEA}$ and $MSNP_{NH3}$ had average negative ζ potentials of −24 ± 0.7, −31 ± 0.3, and −26 ± 0.4 mV, respectively (Table S2), which is attributed to the hydroxyl groups of TEOS. Since the nanoparticles exhibited negative charge, loading of dsRNA, which is also negatively charged, becomes challenging. Thus, for the electrostatic interaction of dsRNA with MSNPs, the surface of the nanoparticles were amine functionalized with APTES to confer positive charge. *Amino*-$MSNP_{DEA}$, $MSNP_{TEA}$ and $MSNP_{NH3}$ had average positive ζ potentials of 4 ± 0.2, 4.5 ± 0.2, and 5 ± 0.1 mV, respectively, confirming functionalization onto the nanoparticles (Sapino et al. 2015) (Fig. 2d).

The surface functional groups on the nanoparticles were also characterized by FTIR spectroscopy. Fig S1a shows the FTIR spectra of all three MSNPs before and after amine functionalization. The Si–O–Si peak at 1054 cm^{-1} and Si–O peak at 808 cm^{-1} were clearly detected in all three MSNPs.

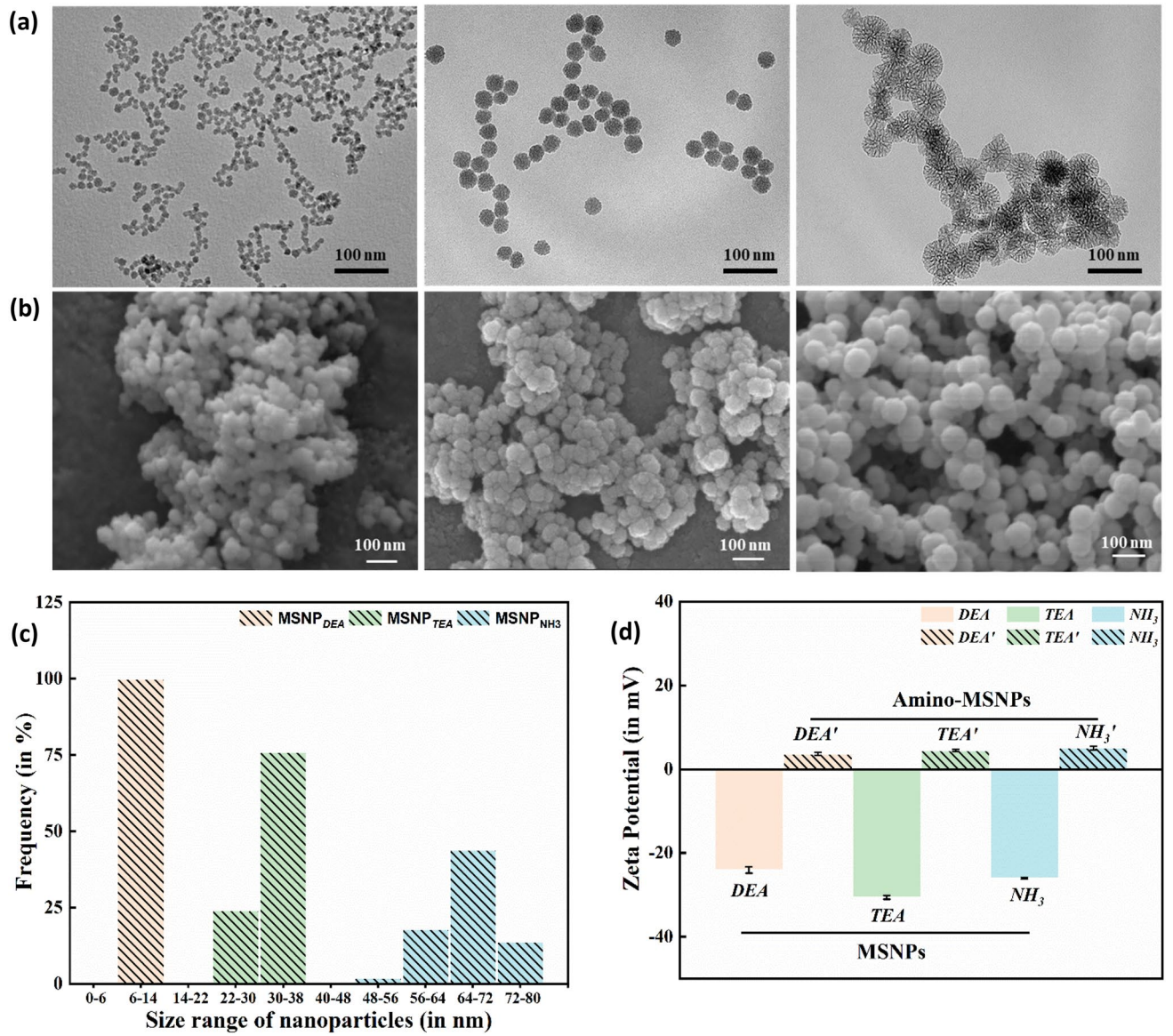

Fig. 1 Characterization of the mesoporous silica nanoparticles. **a** High-resolution transmission electron microscopy images of $MSNP_{DEA}$, $MSNP_{TEA}$ and $MSNP_{NH3}$. **b** Field emission scanning electron microscopy images of $MSNP_{DEA}$, $MSNP_{TEA}$, and $MSNP_{NH3}$. **c** Size distribution of all three nanoparticles calculated by ImageJ software. **d** Zeta potential measurements before and after modification with APTES

The peaks at 960 cm^{-1} belonged to Si–OH groups (Xue et al. 2017). As can be seen from Fig S1a, the absorption peak of CH and CH_2 groups were found at 2931 cm^{-1}. Also, two clear distinctive peaks of NH were observed at 1591 and 1479 cm^{-1} suggesting the successful functionalization on the MSNPs. In addition, a vibration peak at 1314 cm^{-1} due to stretching bands of C–N groups were observed after MSNPs functionalized with amino groups (Meroni et al. 2017).

Figure S1b shows the high angle XRD and 2θ was observed between 10° and 50° for all three MSNPs. A typical peak at 23° was observed in all three nanoparticles, proving that MSNPs have been formed successfully. Fig. S1c shows the low angle powder XRD (LAXRD) plot of all three MSNPs. For $MSNP_{NH3}$ no peak was observed indicating highly random mesopore structure, whereas for $MSNP_{DEA}$ and $MSNP_{TEA}$ has one single low intensity peak suggesting slightly ordered mesopore structure in comparison to $MSNP_{NH3}$ (Zeng and Bai 2014). All three samples did not show second and third peaks, which is generally present in MCM41 type MSNPs (highly ordered mesopores), proving the random mesopore structure in all three nanoparticles (Zhang et al. 2012). Figure S1d shows the double-logarithmic plot generated from SAXS patterns of MSNPs. None of the scattering curves in the plot

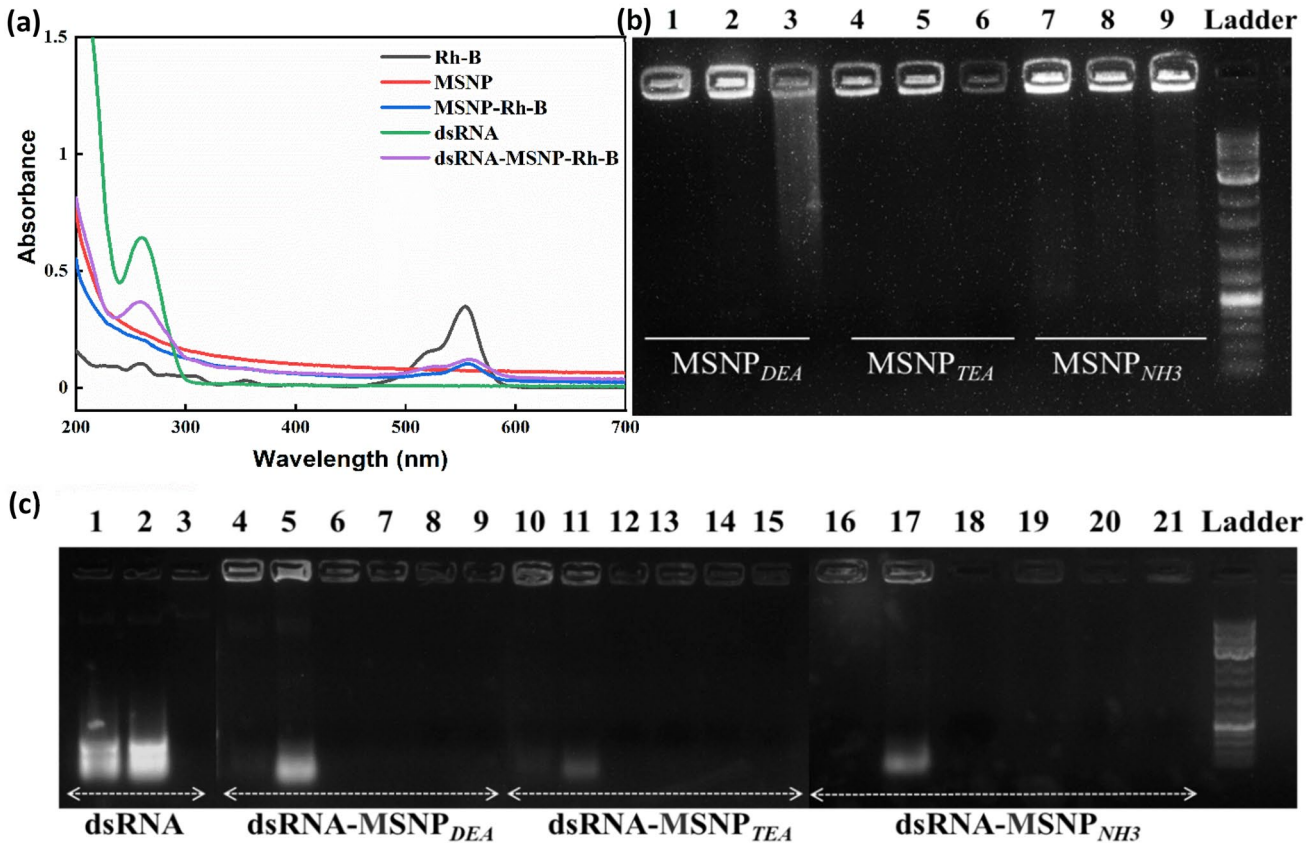

Fig. 2 **a** Absorbance spectra of Rh-B (black), MSNP (red), MSNP-Rh-B (blue), dsRNA (green) and dsRNA-MSNP-Rh-B (purple). **b** Electrophoretic mobility pattern of all three dsRNA/MSNP complexes from left to right into different dsRNA/MSNP weight ratios; 1:10 (well 1, 4, 7 for MSNP$_{DEA}$, MSNP$_{TEA}$ and MSNP$_{NH3}$), 1:6.67 (well 2, 5, 8), 1:5 (well 3, 6, 9) on agarose gel. **c** RNase protection capacity for dsRNA-*amino*-MSNPs: wells from left to right: naked dsRNA (well 1), naked dsRNA treated with Heparin (well 2), naked dsRNA treated with RNase A (10 µg/µl, for 20 min) (well 3) dsRNA-loaded-*amino*-MSNPs (well 4, 10, 16), heparin treated dsRNA-*amino*-MSNPs in the absence of the RNase A (well 5, 11, 17), dsRNA-*amino*-MSNPs in the presence of the RNase for 20 min (well 6, 12, 18), for 40 min (well 7, 13, 19), for 60 min (well 8, 14, 20), and finally 120 min (well 9, 15, 21)

showed interference maxima, thus again confirming the random structure of mesopores in all three nanoparticles (Stoeckel et al. 2014). N_2 Adsorption isotherms showed type IV N_2 adsorption isotherm for all three samples, confirming the mesoporosity in nanoparticles (Fig. S2).

Characterization of Rh-B tagged MSNPs, surface coating and dsRNA conjugation

The absorbance spectrum of the untagged MSNPs and Rh-B-tagged MSNPs were studied not only to confirm the presence of dye but also to estimate loading of dsRNA (Fig. 2a). The results showed that MSNPs themselves have no evident absorption peak in the UV–vis region. After loading with Rh-B, the complex has a noticeable characteristic absorption peak at 554 nm. The presence of Rhodamine B in the MSNPs allows their intracellular detection into the leaves and roots. After loading with Rh-B and encapsulating with dsRNA after amine modification, the complex not only had an obvious characteristic absorption peak at 554 nm due to the dye but also showed a peak at 260 nm, corresponding to dsRNA. The spectra thus indicate the simultaneous presence of both Rh-B and dsRNA, confirming the successful Rh-B tagging and dsRNA conjugation.

Gel retardation assay and dsRNA conjugation efficiency

Negatively charged dsRNA was attached by electrostatic interaction to the positively charged *amino*-MSNPs by incubation (Ma et al. 2013). To determine the complex formation of dsRNA with *amino*-MSNPs, a gel retardation assay was conducted after incubation. Once dsRNA was bound to the MSNPs, mobility of dsRNA was retarded because of the large size of the nanoparticles and the samples did not show any movement and was retained in the gel wells. We investigated the dsRNA conjugation efficiency

in three different dsRNA concentrations; 100 µg/mg, 150 µg/mg and 200 µg/mg of nanoparticles. Figure 2b shows that all three dsRNA concentrations showed efficient binding with *amino*-MSNPs, but more effectively in the ratio 1:6.67 (lane 2, 5, 8), as evident by gel electrophoresis. dsRNA conjugation efficiency (CE%) of *amino*-$MSNP_{DEA}$, *amino*-$MSNP_{TEA}$ and a*mino*-$MSNP_{NH3}$, was found to be $46 \pm 0.8\%$, $65 \pm 5\%$ and $71 \pm 5\%$. The variations in dsRNA conjugation efficiency among the a*mino*-MSNPs might be because of the intrinsic differences in sizes and charges, which possibly influence the mechanism of interaction involving dsRNA cargos and different a*mino*-MSNP carriers.

Stability of dsRNA loaded onto MSNPs

For dsRNA–MSNPs to offer RNAi-facilitated protection against viral pathogens, dsRNA should not only stay on the surface of leaves for a long period than free dsRNA but should also resist nuclease degradation as enzymatic cleavage of naked dsRNA in the environment is a significant barrier in effective gene delivery. Loading the dsRNA in nanoparticles offers protection to the nucleic material from degradation. Thus, for accessing the nano-conjugate's applicability in achieving RNAi, we next checked for the stability of dsRNA loaded in a*mino*-MSNPs in the presence of RNase A. We incubated either free dsRNA or dsRNA-MSNPs with RNase A at 37 °C for 20, 40, 60, and 90 min. To examine the nucleases protecting effect of nanoparticles on dsRNA, the incubated samples were run on a 1.2% of agarose gel to check intact versus degraded dsRNA. It was observed that silencing naked dsRNA was totally digested, as seen from the absence of an dsRNA band in lane 3 (Fig. 2c), while the dsRNA-loaded onto the three a*mino*-MSNPs remained in the gel wells suggesting significant protection being offered by the MSNP loading from RNase degradation at all time points of; 20 min (lane 6, 12, 18), 40 min (lane 7, 13, 19), 60 min (lane 8, 14, 20) and 90 min (lane 9, 15, 21) (Fig. 2c). The stability of dsRNA–MSNP complexes in presence of heparin sodium salt was assessed by adding heparin solution for 2 min to pre-formed complex solution. Heparin, because of its negative charge is frequently used in competition with dsRNA to bind positively charged vectors and used in dsRNA/siRNA release studies from nanoparticles. Lane 5, 11 and 17 showed dsRNA release from *amino*-MSNPs (Fig. 2c) due to easy displacement of dsRNA by heparin. $MSNP_{TEA}$ exhibited a higher resistance to heparin displacement (lane 11—less intense band than 5 and 17), compared to other two dsRNA–MSNP complexes. The bound dsRNA in all *amino*-MSNP samples remained in the gel wells following RNase-A treatment, clearly demonstrating that *amino*-MSNPs can provide excellent protection to dsRNA from nuclease degradation.

Uptake and translocation of MSNPs into mature plant leaves and roots

After confirming the physical and chemical characteristics, cargo loading efficiency and dsRNA protection ability of the MSNPs, we next assessed the uptake and translocation of the amino-MSNPs into the Nb plant leaf and root using fluorescence microscopy. The plant leaf and root after inoculation with nanoparticles were washed thoroughly and studied for the internalization of all three types of MSNPs into plant cells (Fig. 3).

Nanoparticle uptake in root cells—in these plant uptake and translocation studies, three different delivery methods were used. Briefly, 0.5 mg/mL NP suspension either introduced by rub inoculation, spray application on leaves and into roots by soaking into MSNPs suspension. The presence of rhodamine B or FITC in the MSNPs allows their intracellular detection into leaves and roots by simply observing under fluorescence microscope. As can be seen from the Fig. 3a, b and Fig. S5, uptake of all three MSNPs into the plant root cells were observed, suggesting that functionalized nanoparticles are a good carrier for plant cell internalization. As can be seen in Fig. S5, after 1 h, roots treated with Rhodamine B tagged $MSNP_{DEA}$ (~ 10 nm) and $MSNP_{TEA}$ (~ 32 nm) solution showed strong red fluorescence in comparison to $MSNP_{NH3}$ (~ 66 nm), suggesting efficient intracellular localization, indicating better local cellular uptake. In Fig. 3a, the fluorescent nanoparticles (FITC-tagged) were mainly observed around the cortex region and into the xylem cells of the root cross-sections. To further examine the localization of MSNP at sub-cellular levels, transmission electron microscopy was used. 1 h, post treatment, sections of the roots were examined under the TEM. Representative images of the N.b. plants show accumulation of MSNPs in the intercellular region of the root cells, but in different quantities. The smallest size ($MSNP_{DEA}$) was observed to be internalized the most within one hour of incubation. The possible reason for the low internalization efficiency of $MSNP_{NH3}$ might be its large size that restricts its uptake.

Root-to-leaf translocation—the root experiment has also been re-performed with FITC labelled nanoparticles. We used FITC in place of rhodamine B in translocation experiments, because rhodamine fluorescence is similar to the red autofluorescence emitted by the chloroplasts, using it as a fluorescent marker in plant roots is more advantageous than using it in leaves. Furthermore, these fluorescent labelled MSNPs may be loaded and packed with biomolecules, it is possible to track them to locations where the biomolecule is released. The cross-sections of N.b. stem and leaf petioles after incubation of one hour with roots, was examined under the FITC channel of fluorescence microscopy to locate the accumulation of MSNP-FITC

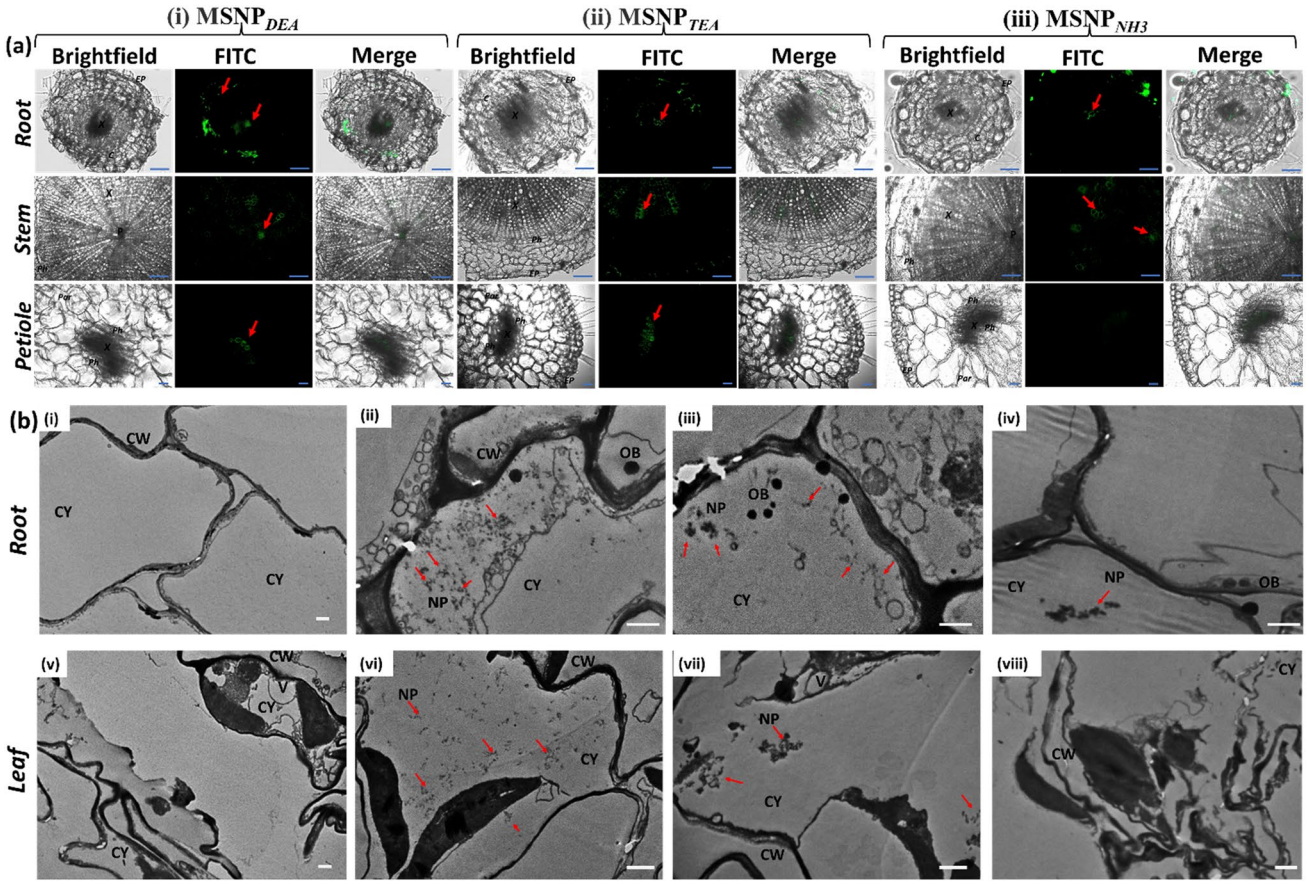

Fig. 3 Accumulation of MSNPs by *Nicotiana benthamiana*. **a** The uptake of fluorescent MSNP-FITC by N.b. root, stem and petiole were analyzed under the bright field and green channel using fluorescence microscopy. (i) Images showing cross-section of N.b. root, stem and petiole treated with MSNP$_{DEA}$, (ii) images of root, stem and petiole cross-sections treated with MSNP$_{TEA}$, and (iii) images showing cross-section of N.b. root, stem and petiole treated with MSNP$_{NH3}$. Where *x* xylem, *Ph* phloem, *c* cortex, *ep* epidermis, and *par* parenchymatic cells. Red arrows indicate presence of FITC labelled MSNPs. Scale bar 50 µm. The images are representatives of experimental replicates ($n=3$). **b** Transmission electron microscopy images of roots from (i) blank solution, (ii) treated with MSNP$_{DEA}$, (iii) treated with MSNP$_{TEA}$ and (iv) treated with MSNP$_{NH3}$. TEM images of leaves from (v) blank solution, (vi) treated with MSNP$_{DEA}$, (vii) treated with MSNP$_{TEA}$, and (viii) treated with MSNP$_{NH3}$. Red arrows indicate MSNPs. Where *CW* cell wall, *CY* cytoplasm, *OB* oil bodies, *V* vacuole and *NP* nanoparticles. Scale bars are defined in each image is 1 µm

in different cell types. As can be seen in Fig. 3a, the assessment of stem and leaf petiole cross-sections resulted in the accumulation of fluorescent nanoparticles in the endodermis and xylem of the stem, and were transported through the vascular tissue to the petiole of the leaves. All three amino-MSNPs were efficiently internalized, although in different quantities by cells as evident by strong green fluorescence. After 1 h of incubation, MSNPs movement has been observed around the cortex via apoplastic pathways, ultimately entering into the plant vascular bundle (xylem), translocated into above ground organs via ascent of sap in xylem. However, MSNP$_{DEA}$ and MSNP$_{TEA}$ led to a significantly higher fluorescence in root, stem and petiole sections of the plant than that of MSNP$_{NH3}$ after 1 h of exposure, indicating small size leads to efficient NP uptake and translocation. No fluorescence has been observed into petiole sections of the plants treated with MSNP$_{NH3}$. Fluorescence data further confirmed the observations made by transmission electron microscopy analysis. The resulting TEM images revealed that the MSNP$_{DEA}$ and MSNP$_{TEA}$ were observed into the leaf cells of the *N. benthamiana*. However, fewer nanoparticles were seen with increasing particle size (MSNP$_{TEA}$) because of the inability of the higher sizes to enter into the cells as quickly. No nanoparticles were visible in the leaves treated with MSNP$_{NH3}$ (but fewer has been observed in the root sections), which is similar to the observation made by the fluorescence microscopy. The data clearly indicates that a critical size of nanoparticles (< 50 nm) plays a key role in transporting through plants.

Leaf-to-leaf translocation—furthermore, following incubation time of 1-day post-infiltration (dpi) of leaf, fluorescence microscopy was performed on the rub

inoculated leaf tissues and the systemic movement of FITC fluorescence due to the presence of nanoparticles was detected in the non-applied adjacent leaf petioles of nano-conjugate treated plants (Fig. S8). These observations imply that MSNPs can be internalized in plant cells and translocate to different sites in plant via xylem conduit in petioles and midrib sections of the leaves. The MSNP-FITC mainly located in the xylem channels of the petiole of treated and untreated leaves. Thus, translocation from a leaf to other parts of the plant most likely due to capillary forces and vasculature flow. Also evident was the high concentrations of small sized (~ 10 nm) MSNPs in the system by all three inoculation methods. In contrast, all the sizes showed significant translocation to the untreated leaf except the $MSNP_{NH3}$ which showed negligible fluorescence in the untreated leaf petioles.

Also, to check the nanoparticle foliar delivery efficiency, plants leaves were sprayed with all three nanoparticles and kept in incubation for 4 h (Fig. 4). Nanoparticles size < 50 nm has been seen translocating across the nicotiana leaf surface around the epidermal cell boundaries along with stomatal complex. In contrast, stomata were the main pathway of entry for the $MSNP_{NH3}$ (> 50 nm) nanoparticles into the leaves, highlighting the potential differences of NP translocation between various sizes. The efficient foliar delivery of the nanoparticles on leaves may also be affected by the adhesion ability of the NPs on leaf surface. This observation can be attributed to the fact that large NPs are more easily washed away than smaller ones (Avellan et al. 2019; Kah et al. 2019).

Efficacy analysis of ds-*AC2* conjugated MSNPs against ToLCNDV

The efficacy of topically applied dsRNA for providing protection against ToLCNDV were assessed by symptom development in local and systemic leaves. After 11-day post-inoculation, the average disease incidence observed in the control plants (treated with ToLCNDV) was 65.7%. All plants treated with dsRNA showed disease suppression in comparison to the control. The disease incidence was significantly lower in plants treated with dsRNA–$MSNP_{DEA}$ (25.71%) and dsRNA-$MSNP_{TEA}$ (14.28%) compared to the plants treated with dsRNA–$MSNP_{NH3}$ (34.28%) and

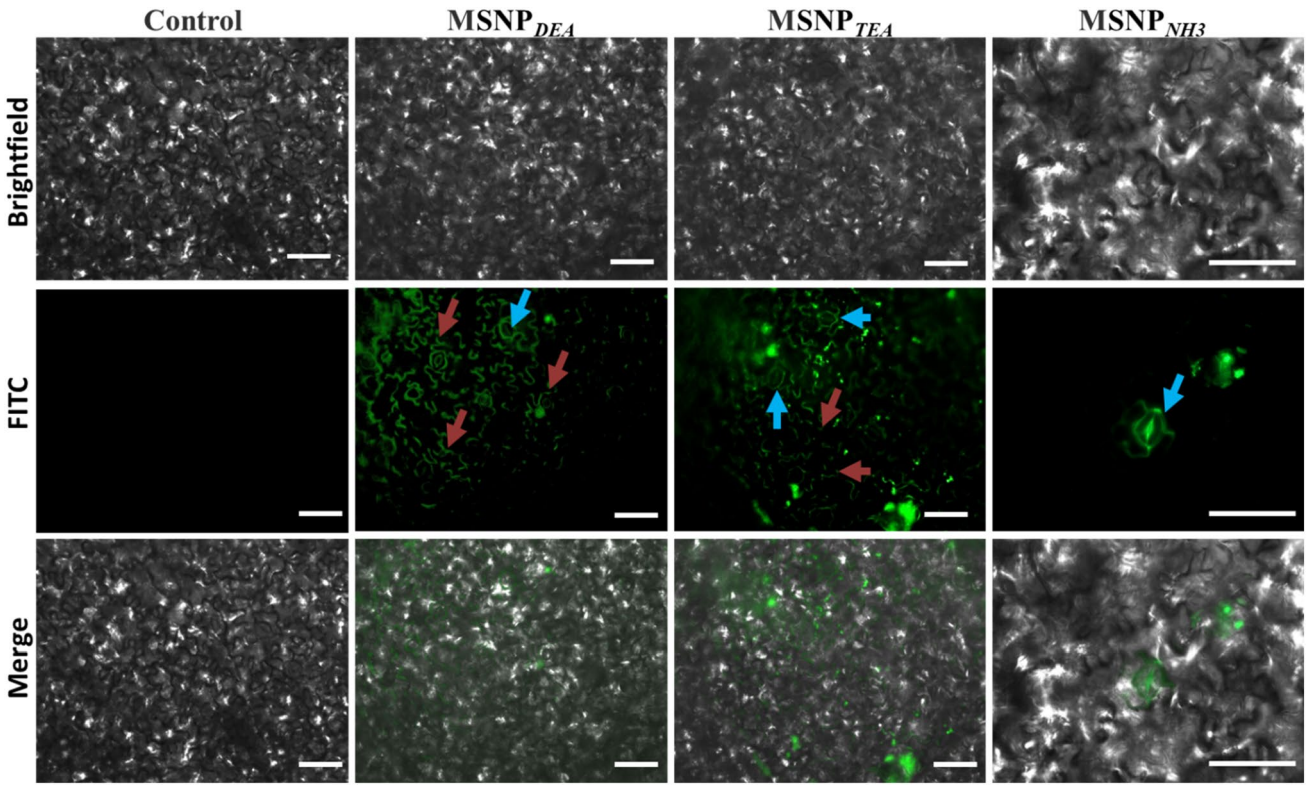

Fig. 4 Comparison of foliar delivery of different MSNPs into plant leaves. Images were collected after 4 h of incubation with MSNPs. Representative fluorescence microscopy images of the leaf epidermal cells indicating translocation of $MSNP_{DEA}$ and $MSNP_{TEA}$, around the epidermal cell boundaries along with stomatal complex. In contrast, stomata were the main pathway of entry for the $MSNP_{NH3}$ nanoparticles into the leaves, highlighting the potential differences of NP translocation between various sizes. Cyan arrows and orange arrows indicate extracellular space and stomatal guard cells, respectively. The images are representatives of experimental replicates ($n = 3$).

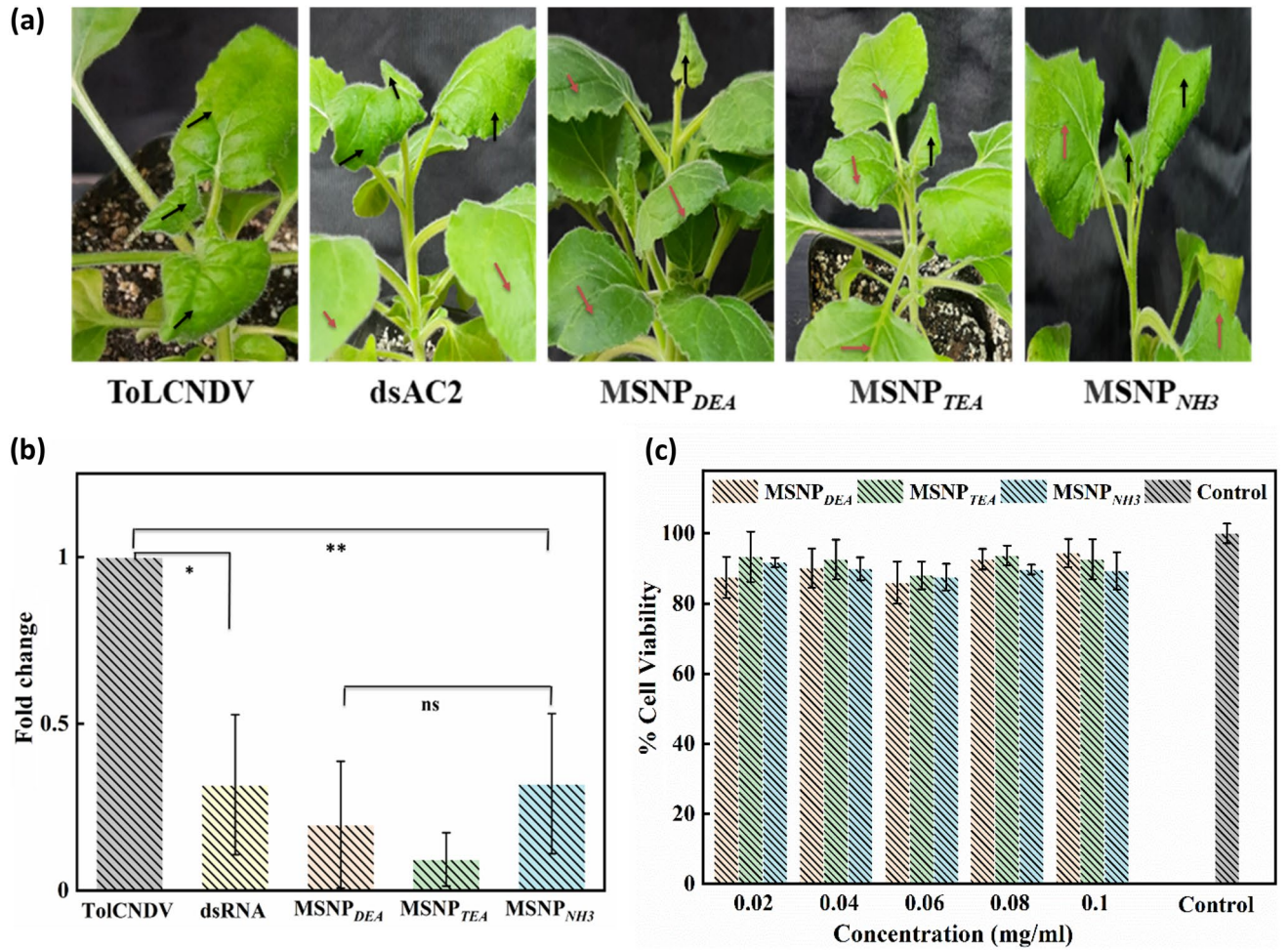

Fig. 5 **a** Efficacy assay of *dsAC2* in *N. benthamiana* (i) Showing reduction of symptoms in *dsAC2* treated *N. benthamiana* after challenge inoculation with infectious construct of ToLCNDV at 11dpi (black and red arrows shows elevated and reduced leaf curling symptoms). **b** qPCR showing significant reduction of ToLCNDV load at 6-day postinfiltration in all the three-dsRNA loaded Amino-MSNPs, with ToLCNDV inoculated (control), naked dsRNA, and dsRNA-loaded MSNPs {(*$p \leq 0.05$ **$p \leq 0.01$, in one-way ANOVA, ns denotes not significant, and error bars indicate sem ($n = 3$)}. Three independent experiments were analyzed using AV2 gene as endogenous reference control. **c** To check for the cytotoxicity of nanoparticles, MTT Assay was performed at different concentrations i.e., 0.02, 0.04, 0.06, 0.08 and 0.1 mg/ml of all three nanoparticles and error bars indicate SD ($n = 3$)

dsRNA alone (42.85%) (Fig. 5a and Fig. S6). Furthermore, viral load in dsRNA-treated and non-treated leaf were quantified using real-time PCR. The apical leaves from treated plants were taken for DNA extraction at different intervals of time; day 6, 18 and 30th and viral titres were assessed by qPCR. The qPCR analysis from the systemic leaves showed a significant decrease in viral load in all plants applied with naked dsRNA and dsRNA-MSNPs. We found that MSNP$_{NH3}$ (3-fold reduction) did not exhibit any significant decrease in viral load relative to plants delivered with free naked dsRNA (3-fold reduction), i.e., may be because of large size of nanoparticle that hindered its uptake and translocation, thus affecting viral gene silencing. Whereas the dsRNA delivered by a*mino*-MSNP$_{DEA}$, and *amino*-MSNP$_{TEA}$ demonstrated 5- and 11-folds reduction of ToLCNDV at 6 dpi, respectively (Fig. 5b). As can be seen by uptake experiments, the MSNP$_{DEA}$ has shown better uptake and translocation via all methods of inoculation, but the lesser viral load reduction might be due to low dsRNA loading capacity of MSNP$_{DEA}$ (46%) in comparison to MSNP$_{TEA}$ (65%). The qPCR experiments done at day18 (0.64-, 0.98- and 0.96-fold change in plants treated with *dsAC2*-MSNP$_{DEA}$, *dsAC2*-MSNP$_{TEA,}$ and *dsAC2*-MSNP$_{NH3}$, respectively) and day 30 (0.31-, 0.71- and 0.32-fold change in plants treated with *dsAC2*-MSNP$_{DEA}$, *dsAC2*-MSNP$_{TEA,}$ and *dsAC2*-MSNP$_{NH3}$, respectively) showed an increase in viral load in all treatments. Collectively, the results shows that dsRNAs applied through nanocarriers with sizes < 50 nm significantly suppresses the effects of ToLCNDV infection in contrast to naked dsRNA.

Mammalian cell toxicity evaluation of the MSNPs

The MTT assay revealed that the all three MSNP nanoparticles were well tolerated by fibroblast cell lines and showed excellent cytocompatibility at all concentrations tested (20 to 100 µg/ml) (Fig. 5c). After MTT assay, the cell viability of the MSNPs were studied by live-dead staining. The calcein-AM and PI staining allows qualitative evaluation of membrane integrity and cell morphology. PI cannot be taken up by live cells and usually enter inside the cells via compromised cell membrane, while non-fluorescent calcein-AM is easily penetrated inside the cells by the lipid membrane. The internalized non-florescent calcein-AM gets cleaved by intracellular esterase to a highly fluorescent calcein indicating the viability of cells. All three MSNPs at various concentrations showed no significant cell mortality, as can be clearly seen from the microscopic images (Fig. S4). The green fluorescence due to cleaved calcein was uniformly spread into the cytoplasm and the red fluorescence due to internalized PI was negligible suggesting live and healthy cells.

Discussion

Till date, nanoparticles are used as the carrier of RNAi primarily in the field of human therapeutics with very few studies in plant virus management applications (Bocos-Asenjo et al. 2022; Mitter et al. 2017; Worrall et al. 2019), because of the presence of cell wall presenting a great barrier (Zhang et al. 2021). Numerous unique nanomaterials have been produced and applied in agricultural sciences for the development of pest and pathogen stress tolerance, sustained release of micro-nutrients and passive delivery of nucleic acids. There is not enormous data of potential nanocarriers that can improve dsRNA delivery and help us control the virus expansion and vector transmission. There are several reports where nanoparticle-mediated RNAi has been used in pest management where various engineered nanoparticles are used for RNAi cargo, such as chitosan NPs, AuNPs, carbon dots, LDH nanosheets and mesoporous silica nanoparticles (Edwards et al. 2020; Wang et al. 2020; Castellanos et al. 2019). There is lack of systematic studies of potential nanocarriers that can improve dsRNA delivery and help us in sustainable management of plant viral pathogens. Mitter et al (2017) explored the potential application of LDH nanosheets as a dsRNA carrier (dsRNA against replicase gene of pepper mild mottle virus; 2b suppressor of cucumber mosaic virus) for sustained and efficient protection against plant viruses. In another study by Worrall et al (2019), the group demonstrated that LDH nanosheets with dsRNA against the coding region of nuclear inclusion b (NIb) protein or coat protein (CP) topically applied to *N. benthamiana* and *Vigna unguiculata* plant leaves, challenged with Bean Common Mosaic Virus (BCMV) protected plants against mechanical inoculation with BCMV transmission by *Myzus persicae*.

Various metal NPs include nickel (Ni), platinum (Pt), gold (Au), silver (Ag), and iron have gathered attention as nano-aided agrochemicals, because of their antiviral, antibacterial properties and growing uses in plant pathology (Farooq et al. 2021; Khan et al. 2022). In spite of the advantages, the metal NPs have shown considerable toxicity to the cells particularly at effective concentrations. The biodegradable nature of MSNPs eliminates such issues and facilitate the delivery of dsRNA even at higher doses (our results showed loading up to 1:5 weight ratios of dsRNA/MSNP) or by systemic administration. Moreover, the system could be modified to load several dsRNA sequences to multiplex silencing targets by loading one type of dsRNAs into the MSNP mesopores, later encapsulating another type of dsRNA after modification. Furthermore, MSNP internalization and nucleic acids delivery into plants can be utilized with other non-model species, and hard-to-transform species.

ToLCNDV is a significant constraint to the tomato crop yield particularly, as it triggers one of the major economical diseases affecting tomato all over the world. With this simple and rapid MSNP delivery system, we achieved effective viral knockdown with a low dsRNA-MSNP dose (150 µg/mg), exhibiting high fold reduction of ToLCNDV titer i.e., up to 11, at 6 days after infiltration. In our system, the disease incidence was significantly lowered by up to 14.28% in nanoparticle treated plants compared to the plants treated with naked dsRNA (42.85%). To attain sustained gene silencing for longer durations, re-infiltration of another dsRNA–MSNP dose around 6th day can be done, to achieve maximum antiviral response. This improved protection offered by the MSNPs nanocarriers (sizes < 50 nm) in contrast to naked dsRNA can help in decreased disease severity by efficiently knocking down the associated pathogens.

Thus, knockdown efficiency is affected by two critical factors i.e., the size and the loading capacity of the nanocarriers. Size appears to be one of the key barriers to penetration into the plant tissues. There are reports concerning the maximum dimensions that plants allow for nanoparticles cellular uptake and translocation, often with a size exclusion limit of 40–50 nm (Corredor et al. 2009). The better knockdown efficiency of $MSNP_{TEA}$ is probably due to better internalization into the plant system as observed in the uptake experiments and high loading capacity of $MSNP_{TEA.}$ The size of the MSNP affects their translocation efficiency within plant tissues, whereby larger sized MSNPs experience greater difficulty bypassing biological barriers like the cuticle or epidermal layers to access inner

leaf layers like the mesophyll. Also, the sizes greater than 50 nm finds it tough to cross cell wall in many plant species (Palocci et al. 2017). The ability to control NP uptake in agrochemical applications may be aided by understanding the size exclusion limit imposed by the cell wall. After confirming the enhanced RNAi by the nanoconjugates and identifying the most efficacious delivery vehicle in plants, we studied the effect of these nanoparticles on mammalian cells. Toxicity associated with nanoparticles is one of the biggest concerns of applying nano-vehicles in agriculture research. The cytotoxicity evaluation studies clearly indicate the superior cytocompatibility of the MSNPs. This is also supported by the fact that the nano-vehicles are made from highly environment friendly and biocompatible silica.

Conferring to the above-mentioned advantages, we are convinced about a wide range of delivery applications of our dsRNA–MSNP system. Additionally, to the conventional phyto applications of RNAi, such as virus/disease resistance, amplifying the production of small biosynthetic molecules, and understanding the function of various proteins, MSNP-mediated gene knockdown has a great potential for efficient delivery of other synthetic ribonucleic acids also. Hence, MSNP-mediated nucleic acid delivery is a valuable resource to increase further the phytotechnology applications of nano-based platforms. In this "new era of Nano agrovehicles", these *amino*-MSNPs offers a great potential in transient plant transformations, without transgene integration.

Conclusion

In this present work, we investigated the possibility of utilising amine-functionalized MSNPs as a dsRNA delivery platform in plants to control viral infection. We showed that the internalization efficiency varies depending upon differences in size of *amino*-MSNPs. We further demonstrated that *amino*-MSNPs can be used as dsRNA delivery agents, producing efficient reduction in viral load by shielding it from nucleases degradation. Fluorescence and transmission electron microscopy of the *amino*-MSNPs following application into plant roots showed that, *amino*-MSNPs was taken up and translocated by the plant cells quickly, within 1 h of post-infiltration. Also, translocation from applied leaf to the adjacent leaf tissues was found to be size-specific. Furthermore, our data suggest that positive surface charge of *amino*-MSNPs bestowed by APTES ligands facilitates the adsorption of dsRNA by electrostatic interaction, thus enabling dsRNA uptake into plant cells. In addition, these delivery vehicles were found to be very well tolerated and biocompatible in mammalian cells. Therefore, *amino*-MSNPs can be a promising dsRNA delivery platform for numerous Phyto biotechnology applications. In summary, our data suggest that *amino*-MSNPs is a biocompatible delivery system for dsRNA-mediated viral gene knockdown in plants and could be employed for various plant biotechnological applications.

Supplementary Information The online version contains supplementary material available at https://doi.org/10.1007/s00299-023-03048-z.

Acknowledgements A.S. acknowledges University Grants Commission (UGC), for financial support as research fellowship. N.S. and B.M acknowledge research funding from National Agricultural Science Fund (NASF), ICAR, India (NASF/ABP-7021/2018-19/256). We thank CRF (IITD) for HR-TEM, FE-SEM, FTIR, XRD and SAXS facilities. We specially thank Gurdeep Kaur (TERI Gram) and Dr P.M. Reddy (TERI Gram) for their help in the final revision of the manuscript.

Author contribution statement AS: data curation, methodology, visualization, original draft; DG: methodology, visualization, review and editing, OSW: review and editing; AR: review and editing; SKM: review and editing; BM: conceptualization, visualization, supervision, review and editing; NS: conceptualization, visualization, supervision, review and editing.

Funding This study was supported by the ICAR-National Agricultural Science Fund (Grant No. NASF/ABP-7021/2018-19/256).

Data availability All data generated for this research have been incorporated in the article/Supplementary Files.

Declarations

Conflict of interest The authors declare no conflict of interest.

References

Abdo GG, Zagho MM, Khalil A (2020) Recent advances in stimuli-responsive drug release and targeting concepts using mesoporous silica nanoparticles. Emerg Mater 3:407–425

Avellan A, Yun J, Zhang Y et al (2019) Nanoparticle size and coating chemistry control foliar uptake pathways, translocation, and leaf-to-rhizosphere transport in wheat. ACS Nano 13:5291–5305. https://doi.org/10.1021/acsnano.8b09781

Bailey-Serres J, Parker JE, Ainsworth EA et al (2019) Genetic strategies for improving crop yields. Nature 575:109–118. https://doi.org/10.1038/s41586-019-1679-0

Bocos-Asenjo IT, Niño-Sánchez J, Ginésy M, Diez JJ (2022) New insights on the integrated management of plant diseases by RNA strategies: mycoviruses and RNA interference. Int J Mol Sci 23:9236. https://doi.org/10.3390/ijms23169236

Boualem A, Dogimont C, Bendahmane A (2016) The battle for survival between viruses and their host plants. Curr Opin Virol 17:32–38. https://doi.org/10.1016/j.coviro.2015.12.001

Calil IP, Fontes EPB (2017) Plant immunity against viruses: antiviral immune receptors in focus. Ann Bot 119:711–723. https://doi.org/10.1093/aob/mcw200

Castellanos NL, Smagghe G, Sharma R et al (2019) Liposome encapsulation and EDTA formulation of dsRNA targeting essential genes increase oral RNAi-caused mortality in the Neotropical stink bug *Euschistus heros*. Pest Manag Sci 75:537–548. https://doi.org/10.1002/ps.5167

Corredor E, Testillano PS, Coronado M, et al Nanoparticle penetration and transport in living pumpkin plants : in situ subcellular

identification. BMC Plant Biol 11:1–11. https://doi.org/10.1186/1471-2229-9-45
Dangl JL, Horvath DM, Staskawich BJ (2013) Pivoting the plant immune system. Science (80-) 341:745–751
Darsan Singh JK, Mat Jalaluddin NS, Sanan-Mishra N, Harikrishna JA (2019) Genetic modification in Malaysia and India: current regulatory framework and the special case of non-transformative RNAi in agriculture. Plant Cell Rep 38:1449–1463. https://doi.org/10.1007/s00299-019-02446-6
Das S, Debnath N, Cui Y et al (2015) Chitosan, carbon quantum dot, and silica nanoparticle mediated dsRNA delivery for gene silencing in *Aedes aegypti*: a comparative analysis. ACS Appl Mater Interfaces 7:19530–19535. https://doi.org/10.1021/acsami.5b05232
Demirer GS, Zhang H, Goh NS et al (2020) Carbon nanocarriers deliver siRNA to intact plant cells for efficient gene knockdown. Sci Adv. https://doi.org/10.1126/sciadv.aaz0495
Douglas AE (2018) Strategies for enhanced crop resistance to insect pests. Annu Rev Plant Biol 69:637–660. https://doi.org/10.1146/annurev-arplant-042817-040248
Edwards CH, Christie CR, Masotti A et al (2020) Dendrimer-coated carbon nanotubes deliver dsRNA and increase the efficacy of gene knockdown in the red flour beetle *Tribolium castaneum*. Sci Rep 10:1–11. https://doi.org/10.1038/s41598-020-69068-x
Farooq T, Adeel M, He Z et al (2021) Nanotechnology and plant viruses: an emerging disease management approach for resistant pathogens. ACS Nano 15:6030–6037. https://doi.org/10.1021/acsnano.0c10910
Fiallo-Olivé E, Pan LL, Liu SS, Navas-Castillo J (2020) Transmission of begomoviruses and other whitefly-borne viruses: dependence on the vector species. Phytopathology 110:10–17. https://doi.org/10.1094/PHYTO-07-19-0273-FI
Ghassemi-Golezani K, Abdoli S (2021) Improving ATPase and PPase activities, nutrient uptake and growth of salt stressed ajowan plants by salicylic acid and iron-oxide nanoparticles. Plant Cell Rep 40:559–573. https://doi.org/10.1007/s00299-020-02652-7
Guerrero J, Regedanz E, Lu L et al (2020) Manipulation of the plant host by the Geminivirus AC2/C2 protein, a central player in the infection cycle. Front Plant Sci 11:1–18. https://doi.org/10.3389/fpls.2020.00591
He B, Chu Y, Yin M et al (2013) Fluorescent nanoparticle delivered dsRNA toward genetic control of insect pests. Adv Mater 25:4580–4584. https://doi.org/10.1002/adma.201301201
Jones RAC (2021) Global plant virus disease pandemics and epidemics
Kah M, Tufenkji N, White JC (2019) Nano-enabled strategies to enhance crop nutrition and protection. Nat Nanotechnol 14:532–540. https://doi.org/10.1038/s41565-019-0439-5
Khan MR, Siddiqui ZA, Fang X (2022) Potential of metal and metal oxide nanoparticles in plant disease diagnostics and management: recent advances and challenges. Chemosphere 297:134114. https://doi.org/10.1016/j.chemosphere.2022.134114
Kwak SY, Lew TTS, Sweeney CJ et al (2019) Chloroplast-selective gene delivery and expression in planta using chitosan-complexed single-walled carbon nanotube carriers. Nat Nanotechnol 14:447–455. https://doi.org/10.1038/s41565-019-0375-4
Lei WX, An ZS, Zhang BH et al (2020) Construction of gold-siRNANPR1 nanoparticles for effective and quick silencing ofNPR1 in *Arabidopsis thaliana*. RSC Adv 10:19300–19308. https://doi.org/10.1039/d0ra02156c
Li K, Wu G, Li M et al (2018) Transcriptome analysis of *Nicotiana benthamiana* infected by tobacco curly shoot virus. Virol J 15:1–15. https://doi.org/10.1186/s12985-018-1044-1
Liu C, Tian S, Lv X et al (2022) Nicotiana benthamiana asparagine synthetase associates with IP-L and confers resistance against tobacco mosaic virus via the asparagine-induced salicylic acid signalling pathway. Mol Plant Pathol 23:60–77. https://doi.org/10.1111/mpp.13143
Livak KJ, Schmittgen TD (2001) Analysis of relative gene expression data using real-time quantitative PCR and the 2-ΔΔCT method. Methods 25:402–408. https://doi.org/10.1006/meth.2001.1262
Ma X, Zhao Y, Ng KW, Zhao Y (2013) Integrated hollow mesoporous silica nanoparticles for target drug/siRNA co-delivery. Chem A Eur J 19:15593–15603. https://doi.org/10.1002/chem.201302736
Meroni D, Lo Presti L, Di Liberto G et al (2017) A close look at the structure of the TiO_2–APTES interface in hybrid nanomaterials and its degradation pathway: an experimental and theoretical study. J Phys Chem C 121:430–440. https://doi.org/10.1021/acs.jpcc.6b10720
Miller RNG, Alves GSC, Van Sluys MA (2017) Plant immunity: unravelling the complexity of plant responses to biotic stresses. Ann Bot 119:681–687. https://doi.org/10.1093/aob/mcw284
Mitter N, Worrall EA, Robinson KE et al (2017) Clay nanosheets for topical delivery of RNAi for sustained protection against plant viruses. Nat Plants. https://doi.org/10.1038/nplants.2016.207
Mohan C, Shibao PYT, de Paula FFP et al (2021) hRNAi-mediated knock-down of *Sphenophorus levis* V-ATPase E in transgenic sugarcane (*Saccharum* spp interspecific hybrid) affects the insect growth and survival. Plant Cell Rep 40:507–516. https://doi.org/10.1007/s00299-020-02646-5
Moriones E, Praveen S, Chakraborty S (2017) Tomato leaf curl New Delhi virus: an emerging virus complex threatening vegetable and fiber crops. Viruses. https://doi.org/10.3390/v9100264
Narayan R, Nayak UY (2018) Mesoporous silica nanoparticles : a comprehensive review on synthesis and recent advances. Pharmaceutics. https://doi.org/10.3390/pharmaceutics10030118
Niazian M, Molaahmad Nalousi A, Azadi P et al (2021) Perspectives on new opportunities for nano-enabled strategies for gene delivery to plants using nanoporous materials. Planta 254:1–20. https://doi.org/10.1007/s00425-021-03734-w
Palocci C, Valletta A, Chronopoulou L et al (2017) Endocytic pathways involved in PLGA nanoparticle uptake by grapevine cells and role of cell wall and membrane in size selection. Plant Cell Rep 36:1917–1928. https://doi.org/10.1007/s00299-017-2206-0
Rahman A, Sinha KV, Sopory SK, Sanan-Mishra N (2021) Influence of virus–host interactions on plant response to abiotic stress. Plant Cell Rep 40:2225–2245. https://doi.org/10.1007/s00299-021-02718-0
Sapino S, Ugazio E, Gastaldi L et al (2015) Mesoporous silica as topical nanocarriers for quercetin: characterization and in vitro studies. Eur J Pharm Biopharm 89:116–125. https://doi.org/10.1016/j.ejpb.2014.11.022
Schmittgen TD, Livak KJ (2008) Analyzing real-time PCR data by the comparative CT method. Nat Protoc 3:1101–1108. https://doi.org/10.1038/nprot.2008.73
Sharma N, Prasad M (2020) Silencing AC1 of Tomato leaf curl virus using artificial microRNA confers resistance to leaf curl disease in transgenic tomato. Plant Cell Rep 39:1565–1579. https://doi.org/10.1007/s00299-020-02584-2
Sharma VK, Basu S, Chakraborty S (2015) RNAi mediated broad-spectrum transgenic resistance in *Nicotiana benthamiana* to chilli-infecting begomoviruses. Plant Cell Rep 34:1389–1399. https://doi.org/10.1007/s00299-015-1795-8
Sharma A, Kumar V, Shahzad B et al (2019) Worldwide pesticide usage and its impacts on ecosystem. SN Appl Sci 1:1–16. https://doi.org/10.1007/s42452-019-1485-1
Singh OW, Gupta D, Joshi B et al (2022) Spray application of a cocktail of dsRNAs reduces infection of chilli leaf curl virus in Nicotiana benthamiana. J Plant Dis Prot 129:433–438. https://doi.org/10.1007/s41348-021-00549-5
Stoeckel D, Wallacher D, Zickler GA et al (2014) Coherent analysis of disordered mesoporous adsorbents using small angle X-ray

scattering and physisorption experiments. Phys Chem Chem Phys 16:6583–6592. https://doi.org/10.1039/c3cp55072a
Strange RN, Scott PR (2005) Plant disease: a threat to global food security. Annu Rev Phytopathol 43:83–116. https://doi.org/10.1146/annurev.phyto.43.113004.133839
Sun D, Hussain HI, Yi Z et al (2014) Uptake and cellular distribution, in four plant species, of fluorescently labeled mesoporous silica nanoparticles. Plant Cell Rep 33:1389–1402. https://doi.org/10.1007/s00299-014-1624-5
Tabashnik BE, Carrière Y (2017) Surge in insect resistance to transgenic crops and prospects for sustainability. Nat Biotechnol 35:926–935. https://doi.org/10.1038/nbt.3974
Tarn D, Ashley CE, Xue M et al (2013) Mesoporous silica nanoparticle nanocarriers. Acc Chem Res 46:792
Wang JW, Grandio EG, Newkirk GM et al (2019) Nanoparticle-mediated genetic engineering of plants. Mol Plant 12:1037–1040. https://doi.org/10.1016/j.molp.2019.06.010
Wang K, Peng Y, Chen J et al (2020) Comparison of efficacy of RNAi mediated by various nanoparticles in the rice striped stem borer (*Chilo suppressalis*). Pestic Biochem Physiol. https://doi.org/10.1016/j.pestbp.2019.10.005
Worrall EA, Bravo-Cazar A, Nilon AT et al (2019) Exogenous application of RNAi-inducing double-stranded RNA inhibits aphid-mediated transmission of a plant virus. Front Plant Sci. https://doi.org/10.3389/fpls.2019.00265
Wu SH, Lin HP (2013) Synthesis of mesoporous silica nanoparticles. Chem Soc Rev 42:3862–3875. https://doi.org/10.1039/c3cs35405a
Xue G, Yurun F, Li M et al (2017) Phosphoryl functionalized mesoporous silica for uranium adsorption. Appl Surf Sci 402:53–60. https://doi.org/10.1016/j.apsusc.2017.01.050
Zeng W, Bai H (2014) Swelling-agent-free synthesis of rice husk derived silica materials with large mesopores for efficient CO2 capture. Chem Eng J 251:1–9. https://doi.org/10.1016/j.cej.2014.04.041
Zhang X, Zheng X, Zhang S et al (2012) AM-TEPA impregnated disordered mesoporous silica as CO_2 capture adsorbent for balanced adsorption–desorption properties. Ind Eng Chem Res 51:15163–15169. https://doi.org/10.1021/ie300180u
Zhang H, Cao Y, Xu D et al (2021) Gold-nanocluster-mediated delivery of siRNA to intact plant cells for efficient gene knockdown. Nano Lett 21:5859–5866. https://doi.org/10.1021/acs.nanolett.1c01792
Zotti M, dos Santos EA, Cagliari D et al (2018) RNA interference technology in crop protection against arthropod pests, pathogens and nematodes. Pest Manag Sci 74:1239–1250. https://doi.org/10.1002/ps.4813